Extracting Quantum Many-Body Scarred Eigenstates with Matrix Product States

Shun-Yao Zhang, Dong Yuan, Thomas Iadecola, Shenglong Xu, and Dong-Ling Deng

Phys. Rev. Lett. **131**, 020402 — Published 11 July 2023

DOI: 10.1103/PhysRevLett.131.020402

Extracting Quantum Many-Body Scarred Eigenstates with Matrix Product States

Shun-Yao Zhang,[1,*] Dong Yuan,[1,*] Thomas Iadecola,[2,3,†] Shenglong Xu,[4,‡] and Dong-Ling Deng[1,5,§]

[1]*Center for Quantum Information, IIIS, Tsinghua University, Beijing 100084, People's Republic of China*
[2]*Department of Physics and Astronomy, Iowa State University, Ames, Iowa 50011, USA*
[3]*Ames National Laboratory, Ames, Iowa 50011, USA*
[4]*Department of Physics and Astronomy, Texas A&M University, College Station, Texas 77843, USA*
[5]*Shanghai Qi Zhi Institute, 41st Floor, AI Tower, No. 701 Yunjin Road, Xuhui District, Shanghai 200232, China*

Quantum many-body scarred systems host nonthermal excited eigenstates immersed in a sea of thermal ones. In cases where exact expressions for these special eigenstates are not known, it is computationally demanding to distinguish them from their exponentially many thermal neighbors. We propose a matrix-product-state (MPS) algorithm, dubbed DMRG-S, to extract such states at system sizes far beyond the scope of exact diagonalization. Using this technique, we obtain scarred eigenstates in Rydberg-blockaded chains of up to 80 sites and perform a finite-size scaling study to address the lingering question of the stability for the Néel state revivals in the thermodynamic limit. Our method also provides a systematic way to obtain *exact* MPS representations for scarred eigenstates near the target energy without *a priori* knowledge. In particular, we find several new scarred eigenstates with exact MPS representations in kinetically constrained spin and clock models. The combination of numerical and analytical investigations in our work provides a new methodology for future studies of quantum many-body scars.

Quantum many-body scars (QMBS) appear in many-body systems with weak ergodicity breaking [1–4]. These anomalous scarred eigenstates violate the eigenstate thermalization hypothesis [5–9], yet only comprise a vanishing fraction of the Hilbert space, as opposed to the strong ergodicity breaking in integrable [10] or many-body localized systems [11, 12]. Typical many-body scarred eigenstates possess sub-volume-law entanglement entropy, and are immersed in a sea of thermal eigenstates [see Fig. 1(a)]. Many models exist in which a set of scarred eigenstates can be calculated analytically [13–25], but there are other examples in which their appearance remains mysterious. For instance, experiments in Rydberg-atom quantum simulators realizing the "PXP model" [1, 26] found evidence of QMBS in the dynamics of an initial Néel state, which exhibited coherent revivals for unexpectedly long time owing to its high overlap with a tower of scarred eigenstates. Motivated by these experiments, a flurry of theoretical and experimental works have emerged to explain the rich properties of these special eigenstates [16, 27–38] and find other models hosting many-body scars [30, 39–48].

In such cases without exact analytical expressions for the scarred eigenstates, their existence can be confirmed by full diagonalization of the Hamiltonian followed by a calculation of some diagnostics, e.g. the entanglement entropy, across the whole spectrum. The exponential computational cost of exact diagonalization (ED) poses a substantial challenge to faithfully addressing the fate of QMBS in the thermodynamic limit. Examples of questions that are difficult to address using ED include the ultimate fate of periodic revivals for the Néel state in the PXP model [1, 16] and the robustness of scarred eigenstates under various perturbations [49–52]. Matters can be further complicated by the fact that highly excited eigenstates of many-body Hamiltonians can have exponentially large degeneracy in the presence of certain symmetries [44, 45, 53–55]. This renders the task of finding scars using ED methods extremely difficult in general.

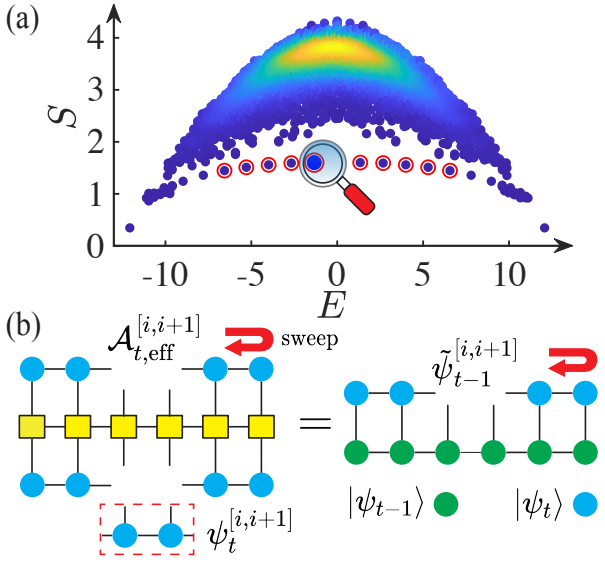

FIG. 1. Schematic illustration of the DMRG-S algorithm for extracting quantum many-body scars with matrix product states. (a) Density plot showing the bipartite entanglement entropy S versus energy eigenvalue E for the PXP model. DMRG-S effectively serves as a magnifier to discover low-entanglement scar states within a target energy window. (b) Schematic of the variational procedure for obtaining the updated matrix product state $|\psi_t\rangle$ (blue circles) from $|\psi_{t-1}\rangle$ (green circles) by locally solving the linear equation $\mathcal{A}_{t,\text{eff}}^{[i,i+1]}\psi_t^{[i,i+1]} = \tilde{\psi}_{t-1}^{[i,i+1]}$, where $\mathcal{A}_t = (H-\xi_t)^2$ (yellow blocks).

Scarred eigenstates in one dimension often have entanglement entropy scaling at most logarithmically with the system size [15, 18, 20, 28, 56], suggesting that they could be described using matrix product state (MPS) representations at system sizes inaccessible to ED [57, 58]. In this paper, we propose an MPS-based algorithm to extract quantum many-body scarred eigenstates with high accuracy (see Fig. 1 for a pictorial illustration). To demonstrate its power, we compute

the tower of scarred eigenstates for system sizes up to $L = 80$ in the PXP model [27, 28] and a deformation thereof [16, 29]. With a detailed finite-size scaling study, we find that the coherent revivals of the Néel state vanish in the thermodynamic limit in the PXP model, whereas they remain stable in the deformed PXP model.

Moreover, previous analytical studies have shown that highly excited scarred eigenstates in several models possess exact MPS representations [15, 17, 20, 54, 59], while the constructions of these scars are model-specific and lack generalizability. In contrast, our method provides a systematic way to find exact MPS representations for QMBS in generic Hamiltonians, without *a priori* knowledge. We use our algorithm to discover several new zero-energy scarred eigenstates with exact MPS representations in the kinetically constrained clock [39] and higher-spin PXP models [30]. We also find *a posteriori* analytical derivations for these scars that apply to a wide variety of kinetically constrained models.

DMRG-S Algorithm.– Our algorithm is inspired by the density matrix renormalization group (DMRG) method [60, 61], which has been widely used to obtain modestly entangled ground states of low-dimensional Hamiltonians. In the past few years, DMRG methods relying on the MPS formalism have been generalized to obtain highly excited eigenstates of many-body localized systems [62–66]. In this work, we modify and improve the shift-invert technique [65–67] to be amenable for calculating scarred eigenstates. Below, we dub the algorithm DMRG-S, where "S" stands for "scars".

The algorithm is based on the intuition that repeatedly applying the inverse operator $(H-\xi)^{-2}$ (more robust and efficient in convergence compared to $(H-\xi)^{-1}$ [68]) to an initial state $|\psi_0\rangle$ eventually yields an eigenstate of H with energy ξ, provided $|\psi_0\rangle$ has overlap with this eigenstate. In practice, we define $|\psi_0\rangle$ to be an MPS and consider the sequence of states $|\psi_t\rangle = \mathcal{N}^{-1}\mathcal{A}_t^{-1}|\psi_{t-1}\rangle$, where $\mathcal{A}_t = (H-\xi_t)^2$ and $\mathcal{N}$ is a normalization factor (We describe an update procedure for ξ_t below). The state $|\psi_t\rangle$ is taken to be an MPS with bond dimension $\chi \leq \chi_{\max}$. Restricting $\chi_{\max}$ to relatively small values effectively serves as a filter for states with low entanglement entropy. In the iteration step t, we circumvent the difficulty of calculating the inverse operator $\mathcal{A}_t^{-1}$ by variationally optimizing $|\psi_t\rangle$ such that $\langle\psi_t|\mathcal{A}_t|\psi_t\rangle = \mathcal{N}^{-1}\langle\psi_t|\psi_{t-1}\rangle$. This approach has the advantage that $\mathcal{A}_t$ can be expressed as a matrix product operator. The optimization can be implemented by locally solving the linear equation

$$\mathcal{A}_{t,\text{eff}}^{[i,i+1]}\psi_t^{[i,i+1]} = \tilde{\psi}_{t-1}^{[i,i+1]}, \tag{1}$$

where $\mathcal{A}_{t,\text{eff}}^{[i,i+1]}$ is the local "effective Hamiltonian" for $\mathcal{A}_t$, $\psi_t^{[i,i+1]}$ is the local tensor of $|\psi_t\rangle$ to be updated, and $\tilde{\psi}_{t-1}^{[i,i+1]}$ is the environment tensor of the overlap $\langle\psi_t|\psi_{t-1}\rangle$ [see Fig. 1(b)]. The optimized $\psi_t^{[i,i+1]}$ is substituted back into $|\psi_t\rangle$, which is then brought to the canonical form via singular value decomposition. We perform the local optimization on each pair of sites $[i, i+1]$ sweeping back and forth, similar to the two-site DMRG sweep procedure [60, 61]. During the iterations, we monitor the energy variance $\sigma_H^2 = \langle H^2\rangle - \langle H\rangle^2$ of $|\psi_t\rangle$, which vanishes if and only if $|\psi_t\rangle$ is an eigenstate. Initially we set ξ_0 within the target energy window $[E-\Delta E, E+\Delta E]$, which may not contain the energy of the initial state $|\psi_0\rangle$. After a few iterations, if σ_H^2 reaches a relatively small value (less than 10^{-3}), we then begin to update $\xi_t = \langle\psi_t|H|\psi_t\rangle$ during each iteration. The update of the energy shift ξ_t is crucial for the convergence if we do not *a priori* know the precise locations of scars in the energy spectrum [68]. These two stages correspond to the slow and fast decay regions shown in Fig. 3(b). Eventually we expect $|\psi_t\rangle$ to converge, i.e. $\lim_{t\to\infty}|\langle\psi_{t-1}|\psi_t\rangle|^2 = 1$, and approach to an eigenstate with energy close to the target one.

Tower of scars in PXP models.– The PXP Hamiltonian is the effective Hamiltonian for a chain of spins satisfying the Rydberg blockade constraint, which forbids configurations containing $|\uparrow\rangle_i|\uparrow\rangle_{i+1}$ due to strong nearest-neighbor interactions [1, 69, 70]. It is given by $H_{PXP} = \sum_i P_i X_{i+1} P_{i+2}$, where $P_i = (1-Z_i)/2$ projects onto $|\downarrow\rangle_i$ and X_i, Z_i are Pauli matrices on site i. H_{PXP} is nonintegrable according to studies of its level statistics, and yet hosts a tower of scars supporting the periodic revival dynamics of the Néel state $|Z_2\rangle = |\uparrow\downarrow\uparrow\cdots\downarrow\rangle$ [27, 28]. Numerical simulations of these dynamics observe that the revivals have a decaying envelope, begging the question of whether they persist at late time in the thermodynamic limit. Ref. [16] found that adding a term $\delta H_2 = -h_2\sum_i P_{i-1}X_iP_{i+i}(Z_{i-2}+Z_{i+2})$ with $h_2 = 1/2 - 1/\sqrt{5} \approx 0.053$ makes the periodic revivals nearly perfect due to the emergence of an approximate $su(2)$ algebra. Here, we benchmark the DMRG-S algorithm by computing the tower of scarred eigenstates in the PXP model and its deformation by δH_2.

We initialize the algorithm in the state $|\psi_0\rangle = |Z_2\rangle$, which has predominant overlap with the $L+1$-dimensional tower of scarred eigenstates $\{|\Psi_n\rangle\}_{n=0}^L$ within corresponding energy windows. During the iterations, we set $\chi_{\max} = 1200$ to reach the desired accuracy due to the logarithmic scaling of subsystem entanglement entropy [27, 28] and the periodic boundary conditions. As shown in Fig. 2, DMRG-S successfully extracts the tower of scars in the PXP model up to $L = 80$. The average energy variance σ_H^2 is less than 10^{-6} [68]. To verify that these MPSs indeed capture the scar tower of the PXP Hamiltonian, we calculate their overlap with $|Z_2\rangle$ [Fig. 2(a)], and their bipartite entanglement entropy [68] for different L. Our results yield smooth curves as a function of energy and agree with ED for small system sizes except for a few scars that accidentally hybridize with thermal eigenstates [28, 34], which are further addressed in [68, 71].

We now investigate the quench dynamics of $|Z_2\rangle$ by finite-size scaling beyond the scope of ED using DMRG-S states up to $L = 80$. First, we compute the total overlap between $|Z_2\rangle$ and $\{|\Psi_n\rangle\}_{n=0}^L$ [Fig. 2(b)], and find that $\sum_{n=0}^L|\langle Z_2|\Psi_n\rangle|^2$ decays exponentially with L for the PXP model. In contrast, this quantity remains near unity for the deformed PXP model. The dashed line in Fig. 2(b)

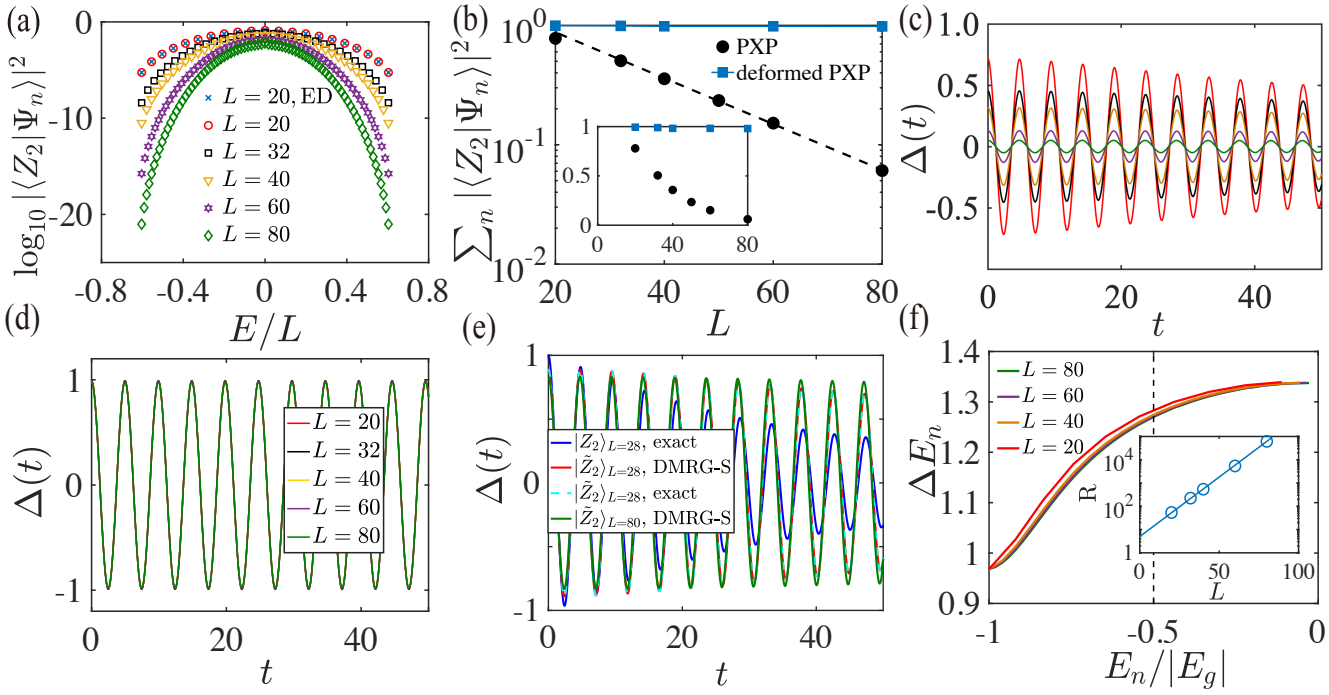

FIG. 2. Numerical results for the tower of scars in the (deformed) PXP model. (a) Overlap between the Néel state $|Z_2\rangle$ and each scarred eigenstate of the PXP model for different L, all obtained by DMRG-S except points marked by crosses. (b) Finite-size scaling for the total overlap between $|Z_2\rangle$ and the $L+1$ scarred eigenstates of the (deformed) PXP model. The inset displays data on the linear scale. (c) Dynamics of the staggered magnetization density Δ within the scarred subspace constructed by DMRG-S ($\mathbb{P}=\sum_{n=0}^{L}|\Psi_n\rangle\langle\Psi_n|$), for the PXP model. (d) The same dynamics for the deformed PXP model. (e) Observable dynamics $\Delta(t)$ of $|\tilde{Z}_2\rangle$ for the PXP model, which exhibits more stable revivals than $|Z_2\rangle$ (blue). $\Delta(t)$ dynamics of $|\tilde{Z}_2\rangle$ computed by using the DMRG-S eigenenergies (red) and by exact Hamiltonian evolution (cyan dashed) agree well with each other. (f) Energy spacings ΔE_n between adjacent scars as a function of the normalized eigenenergy $E_n/|E_g|$ for the PXP model. The inset shows that the ratio R increases exponentially with L.

($y = e^{-0.044L+0.739}$) is obtained from linear regression with $R^2 \approx 0.9996$. To further probe the revivals, we evaluate the dynamics of the staggered magnetization density $\Delta = [\sum_{i=1}^{L}(-1)^{i+1}Z_i]/L$ within the scarred subspace constructed by DMRG-S: $\Delta(t) = \langle Z_2|\mathbb{P}e^{iHt}\Delta e^{-iHt}\mathbb{P}|Z_2\rangle \approx \sum_{n,m=0}^{L} e^{i(E_n-E_m)t}\langle Z_2|\Psi_n\rangle\langle\Psi_n|\Delta|\Psi_m\rangle\langle\Psi_m|Z_2\rangle$, where $\mathbb{P}=\sum_{n=0}^{L}|\Psi_n\rangle\langle\Psi_n|$, $\{E_n\}_{n=0}^{L}$ and $\{|\Psi_n\rangle\}_{n=0}^{L}$ are scarred eigenenergies and eigenstates obtained via DMRG-S [72]. $\Delta(t)$ characterizes the late-time non-thermal observable dynamics after the local relaxation time (the infinite-temperature value of Δ is zero). Fig. 2(c) and (d) display $\Delta(t)$ as a function of time for different L in the PXP and deformed PXP models, respectively. We find that the oscillation amplitude shrinks with increasing L for the PXP model but remains unaltered for the deformed case, consistent with our results for the total $|Z_2\rangle$ overlap.

Furthermore, we evaluate the observable dynamics of the deformed Z_2 state $|\tilde{Z}_2\rangle = \mathbb{P}|Z_2\rangle/\sqrt{\langle Z_2|\mathbb{P}|Z_2\rangle}$ constructed by DMRG-S (which has logarithmic entanglement [68]) in the PXP model. As shown in Fig. 2(e), oscillations of $\Delta(t) = \langle\tilde{Z}_2|e^{iHt}\Delta e^{-iHt}|\tilde{Z}_2\rangle$ become more stable as system size increases, suggesting the robustness of the periodic revivals for $|\tilde{Z}_2\rangle$ in the thermodynamic limit. To illustrate this phenomenon, we calculate the energy spacings ΔE_n between adjacent scars as a function of $E_n/|E_g|$ [Fig. 2(f)], where E_g is the ground state energy and $n = 0, 1, \cdots, L/2$ label the scars from the spectrum boundary to center. Notably, we find that ΔE_n approaches an L- and n-independent constant near the center of spectrum ($E = 0$). Furthermore, inspired by Fig. 2(a), we compute the ratio $R = \sum_{n\in C}|\langle Z_2|\Psi_n\rangle|^2/\sum_{n\in B}|\langle Z_2|\Psi_n\rangle|^2$, where the vertical dashed line $E_n/|E_g| = -0.5$ in Fig. 2(f) separates $|\Psi_n\rangle$ belonging to the spectrum center (C) or boundary (B). As shown in the inset of Fig. 2(f), R increases exponentially with the system size. Combining these two observations, we deduce that the equidistant scars near the center of spectrum dominate the revival dynamics of $|\tilde{Z}_2\rangle$ as L increases, resulting in the more stable oscillations observed in Fig. 2(e).

To sum up, for the PXP model the coherent revivals of the Néel state vanish in the thermodynamic limit due to its exponentially small overlap with the scarred subspace, whereas the revivals remain stable in the deformed case. Nevertheless, our results demonstrate that one can stabilize the revivals in the original PXP model by initializing in a modestly entangled state like $|\tilde{Z}_2\rangle$. The DMRG-S algorithm provides a convenient method to construct such states [68].

Exact MPS representations for QMBS.– Apart from the ability to extract QMBS at system sizes beyond the scope of

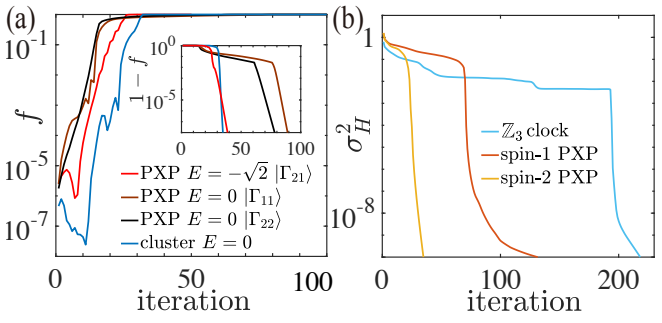

FIG. 3. (a) Fidelity $f = |\langle\psi_t|\Psi_{\text{exact}}\rangle|$ between the optimized MPSs and exact scars from the spin-1/2 PXP model [17] and the deformed one-dimensional cluster model [19] as a function of iteration number. The inset shows the infidelity $1-f$. (b) Energy variance σ_H^2 of the optimized MPSs for the $\mathbb{Z}_3$ clock and spin-1 and 2 PXP models as a function of iteration number.

ED, our algorithm also opens up a promising avenue to naturally obtain the exact MPS representations for certain QMBS. Several exact scars have been discovered in previous analytical studies, such as the $E = \pm\sqrt{2}$ scars $|\Gamma_{12}\rangle, |\Gamma_{21}\rangle$ and the $E = 0$ scars $|\Gamma_{11}\rangle, |\Gamma_{22}\rangle$ in the spin-1/2 PXP model [17], and the $E = 0$ scar in the deformed one-dimensional cluster model [19]. We first benchmark our algorithm by recovering the above known examples. We run the DMRG-S algorithm for about 200 random initial states and select the converged MPS with smallest variance σ_H^2. During the optimization we fix $\chi_{\max} = 10$. As shown in Fig. 3(a), even though the fidelity $f = |\langle\psi_t|\Psi_{\text{exact}}\rangle|$ is initially exceedingly small ($\sim 10^{-6}$), DMRG-S can extract these exact scarred eigenstates to high precision within 100 iterations. We stress that our algorithm is not hindered by the exponentially large degeneracy in the $E = 0$ eigensubspace [53–55] and does not utilize any *a priori* knowledge. Thus it can be applied to generic many-body Hamiltonians in any target energy window.

Indeed, in the kinetically constrained clock model [39] and higher-spin PXP models [30], we discover several $E = 0$ scarred eigenstates with exact MPS representations that have not been reported in previous literature. As shown in Fig. 3(b), the energy variance of the optimized MPSs in the corresponding models converges to very small values ($\sim 10^{-10}$) within 200 iterations. We further apply the singular value decomposition to compress their bond dimensions, typically to $\chi = 2$ for the open boundary cases, then continue the optimization until convergence again. Careful analysis of the bulk tensors on each site yields the expressions reported below. We write the MPS representations as $|\Psi\rangle = \sum_\sigma \text{Tr}\left(A_1^{[\sigma_1]} A_2^{[\sigma_2]} \cdots A_L^{[\sigma_L]}\right) |\sigma_1\sigma_2\cdots\sigma_L\rangle$ for periodic boundary conditions, where $\sigma = \sigma_1\sigma_2\cdots\sigma_L$ denotes the physical index of each site. We define the following 2×2 matrices:

$$B = \begin{pmatrix} 1 & 0 \\ 0 & 0 \end{pmatrix}, \quad D = \begin{pmatrix} 1 & 1 \\ -1 & -1 \end{pmatrix}. \tag{2}$$

These matrices are related to those found in the numerical calculations by appropriate MPS gauge transformations [57, 58].

For the kinetically constrained $\mathbb{Z}_N$ clock model [39] $H_{\text{clock}} = \sum_i P_{i-1} C_i P_{i+1}$, the local Hilbert space is spanned by N states $\{|0\rangle, |1\rangle, \cdots, |N-1\rangle\}$. Here, $P_i = |0\rangle_i \langle 0|_i$ forbids creating excitations (i.e., basis states besides $|0\rangle$) on neighboring sites, and $\mathcal{U}_i = \exp(-iC_i) = \sum_{n=0}^{N-1} |n+1\rangle_i \langle n|_i$ cyclically permutes basis states on site i (we define $|N\rangle \equiv |0\rangle$). A translationally invariant highly excited eigenstate $|\Psi\rangle_c$ with $E = 0$ can be constructed using $A^{[0]} = B$, $A^{[1],[2],\cdots,[N-1]} = D$. In [68] we show that $P_{i-1} C_i P_{i+1} |\Psi\rangle_c = 0$, $\forall\ i$. We further observe that this MPS is nothing but the equal-weight superposition of all computational basis states allowed by the constraints $|\Psi\rangle_c = \sum_{\text{allowed } \sigma} |\sigma_1\sigma_2\cdots\sigma_L\rangle$.

The spin-s PXP models [30] are defined by $H_{PXP} = \sum_i P_{i-1} S_i^x P_{i+1}$, where the local Hilbert space is spanned by $2s+1$ states $\{|-s\rangle, |-s+1\rangle, \cdots, |s-1\rangle, |s\rangle\}$. $P_i = |-s\rangle_i \langle -s|_i$, and S_i^x is the spin-s generator of rotations around the x-axis. When s is an integer, a translationally invariant scarred eigenstate $|\Psi\rangle_s$ with $E = 0$ can be expressed as

$$A^{[-s]} = B, \quad A^{[-s+2k-1]} = 0, \quad A^{[-s+2k]} = a_k D, \tag{3}$$

where $k = 1, 2, 3, \cdots, s$, and $a_k = \langle m_z = -s+2k | m_x = 0\rangle / \langle m_z = -s | m_x = 0\rangle$ [73]. Similarly, $P_{i-1} S_i^x P_{i+1} |\Psi\rangle_s = 0$, $\forall\ i$ [68]. $|\Psi\rangle_s$ also takes a simple form in the computational basis,

$$|\Psi\rangle_s = \sum_{\text{allowed } \sigma} \left[\prod_{k=1}^{s} (a_k)^{\#\text{ of } -s+2k \text{ in } \sigma}\right] |\sigma_1\sigma_2\cdots\sigma_L\rangle, \tag{4}$$

where the allowed computational basis states contain only local states $\{|-s+2k\rangle\}_{k=0}^{s}$ and the additional prefactors count the number of $|-s+2k\rangle$ states appearing in $|\sigma_1\sigma_2\cdots\sigma_L\rangle$.

The above exact scars can be analytically derived as follows. Consider Hamiltonians of the form $H = \sum_i P_{i-1} h_i P_{i+1}$, where the local Hilbert space is spanned by the bases $\{|0\rangle, |1\rangle, \cdots, |d-1\rangle\}$ and $P_i = |0\rangle_i \langle 0|_i$. We define the projector onto the global constrained Hilbert space as $P = \prod_i (I - \tilde{P}_i \tilde{P}_{i+1})$, where $\tilde{P}_i = I - P_i$. If the single-site operator h_i has a zero mode $|\phi_i\rangle$ (e.g. $\sum_{n=0}^{N-1} |n\rangle_i$ for the clock model, and $|m_x = 0\rangle_i$ for the PXP models of integer spins), the product state $|\Phi\rangle = \prod_i |\phi_i\rangle$ is a zero-energy eigenstate of H. While this state does not satisfy the global constraint defined by P, the projected state $P|\Phi\rangle$ does, and in fact remains a zero-energy eigenstate since $[P, H] = 0$. Since P can be expressed as a matrix product operator with bond dimension $\chi = 2$, the zero-energy scarred eigenstate $P|\Phi\rangle$ becomes an MPS with bond dimension $\chi = 2$. Explicit calculations [68] yield the 2×2 matrices in Eq. (2) and the coefficients in Eq. (3). We stress that this construction is different from the embedding construction of Ref. [13], where the embedded scarred eigenstates are annihilated by certain local projectors P_i rather than the local operators h_i.

Conclusion.– In summary, we have introduced the DMRG-S algorithm to accurately extract quantum many-body scarred

eigenstates. This method can access system sizes far beyond the scope of ED and assist analytical studies in discovering exact MPS representations of new scars for generic Hamiltonians. It also sheds light on other open questions about QMBS, such as their robustness under various types of perturbations [49–52]. The analytical construction of exact scars inspired by our numerical results provides a different mechanism for scar states in models with local kinetic constraints. The synergy between numerical calculations and analytical investigations in our work establishes a promising framework for future studies on quantum many-body scars.

The DMRG-S algorithm is implemented based on the ITensor library [74] in Julia programming language. The source code for the numerical calculations is accessible online [75].

We acknowledge helpful discussions with Luming Duan and He-Ran Wang. We especially thank Zlatko Papić for comments on an earlier version of the manuscript. S.-Y. Z., D. Y., and D.-L. D. acknowledge support from the National Natural Science Foundation of China (Grants No. 12075128), Tsinghua University, and Shanghai Qi Zhi Institute. T.I. acknowledges support from the National Science Foundation through Grant No. DMR-2143635.

* These authors contributed equally to this work.
† iadecola@iastate.edu
‡ slxu@tamu.edu
§ dldeng@tsinghua.edu.cn

[1] H. Bernien, S. Schwartz, A. Keesling, H. Levine, A. Omran, H. Pichler, S. Choi, A. S. Zibrov, M. Endres, M. Greiner, *et al.*, "Probing many-body dynamics on a 51-atom quantum simulator," Nature **551**, 579 (2017).
[2] M. Serbyn, D. A. Abanin, and Z. Papić, "Quantum many-body scars and weak breaking of ergodicity," Nat. Phys. **17**, 675 (2021).
[3] S. Moudgalya, B. A. Bernevig, and N. Regnault, "Quantum many-body scars and hilbert space fragmentation: A review of exact results," Rep. Prog. Phys. (2022).
[4] A. Chandran, T. Iadecola, V. Khemani, and R. Moessner, "Quantum many-body scars: A quasiparticle perspective," Annu. Rev. Condens. Matter Phys. **14**, 443 (2023).
[5] J. M. Deutsch, "Quantum statistical mechanics in a closed system," Phys. Rev. A **43**, 2046 (1991).
[6] M. Srednicki, "Chaos and quantum thermalization," Phys. Rev. E **50**, 888 (1994).
[7] J. M. Deutsch, "Eigenstate thermalization hypothesis," Rep. Prog. Phys. **81**, 082001 (2018).
[8] M. Rigol, V. Dunjko, and M. Olshanii, "Thermalization and its mechanism for generic isolated quantum systems," Nature **452**, 854 (2008).
[9] H. Kim, T. N. Ikeda, and D. A. Huse, "Testing whether all eigenstates obey the eigenstate thermalization hypothesis," Phys. Rev. E **90**, 052105 (2014).
[10] B. Sutherland, *Beautiful models: 70 years of exactly solved quantum many-body problems* (World Scientific, 2004).
[11] R. Nandkishore and D. A. Huse, "Many-body localization and thermalization in quantum statistical mechanics," Annu. Rev. Condens. Matter Phys. **6**, 15 (2015).
[12] D. A. Abanin, E. Altman, I. Bloch, and M. Serbyn, "Colloquium: Many-body localization, thermalization, and entanglement," Rev. Mod. Phys. **91**, 021001 (2019).
[13] N. Shiraishi and T. Mori, "Systematic construction of counterexamples to the eigenstate thermalization hypothesis," Phys. Rev. Lett. **119**, 030601 (2017).
[14] S. Moudgalya, S. Rachel, B. A. Bernevig, and N. Regnault, "Exact excited states of nonintegrable models," Phys. Rev. B **98**, 235155 (2018).
[15] S. Moudgalya, N. Regnault, and B. A. Bernevig, "Entanglement of exact excited states of affleck-kennedy-lieb-tasaki models: Exact results, many-body scars, and violation of the strong eigenstate thermalization hypothesis," Phys. Rev. B **98**, 235156 (2018).
[16] S. Choi, C. J. Turner, H. Pichler, W. W. Ho, A. A. Michailidis, Z. Papić, M. Serbyn, M. D. Lukin, and D. A. Abanin, "Emergent su(2) dynamics and perfect quantum many-body scars," Phys. Rev. Lett. **122**, 220603 (2019).
[17] C.-J. Lin and O. I. Motrunich, "Exact quantum many-body scar states in the rydberg-blockaded atom chain," Phys. Rev. Lett. **122**, 173401 (2019).
[18] M. Schecter and T. Iadecola, "Weak ergodicity breaking and quantum many-body scars in spin-1 xy magnets," Phys. Rev. Lett. **123**, 147201 (2019).
[19] S. Ok, K. Choo, C. Mudry, C. Castelnovo, C. Chamon, and T. Neupert, "Topological many-body scar states in dimensions one, two, and three," Phys. Rev. Research **1**, 033144 (2019).
[20] S. Chattopadhyay, H. Pichler, M. D. Lukin, and W. W. Ho, "Quantum many-body scars from virtual entangled pairs," Phys. Rev. B **101**, 174308 (2020).
[21] S. Moudgalya, N. Regnault, and B. A. Bernevig, "η-pairing in hubbard models: From spectrum generating algebras to quantum many-body scars," Phys. Rev. B **102**, 085140 (2020).
[22] K. Lee, R. Melendrez, A. Pal, and H. J. Changlani, "Exact three-colored quantum scars from geometric frustration," Phys. Rev. B **101**, 241111 (2020).
[23] C. M. Langlett, Z.-C. Yang, J. Wildeboer, A. V. Gorshkov, T. Iadecola, and S. Xu, "Rainbow scars: From area to volume law," Phys. Rev. B **105**, L060301 (2022).
[24] C. M. Langlett and S. Xu, "Hilbert space fragmentation and exact scars of generalized fredkin spin chains," Phys. Rev. B **103**, L220304 (2021).
[25] F. Schindler, N. Regnault, and B. A. Bernevig, "Exact quantum scars in the chiral nonlinear luttinger liquid," Phys. Rev. B **105**, 035146 (2022).
[26] D. Bluvstein, A. Omran, H. Levine, A. Keesling, G. Semeghini, S. Ebadi, T. T. Wang, A. A. Michailidis, N. Maskara, W. W. Ho, *et al.*, "Controlling quantum many-body dynamics in driven rydberg atom arrays," Science **371**, 1355 (2021).
[27] C. J. Turner, A. A. Michailidis, D. A. Abanin, M. Serbyn, and Z. Papić, "Weak ergodicity breaking from quantum many-body scars," Nat. Phys. **14**, 745 (2018).
[28] C. J. Turner, A. A. Michailidis, D. A. Abanin, M. Serbyn, and Z. Papić, "Quantum scarred eigenstates in a rydberg atom chain: Entanglement, breakdown of thermalization, and stability to perturbations," Phys. Rev. B **98**, 155134 (2018).
[29] V. Khemani, C. R. Laumann, and A. Chandran, "Signatures of integrability in the dynamics of rydberg-blockaded chains," Phys. Rev. B **99**, 161101 (2019).
[30] W. W. Ho, S. Choi, H. Pichler, and M. D. Lukin, "Periodic orbits, entanglement, and quantum many-body scars in constrained models: Matrix product state approach," Phys. Rev. Lett. **122**, 040603 (2019).
[31] A. A. Michailidis, C. J. Turner, Z. Papić, D. A. Abanin, and

M. Serbyn, "Slow quantum thermalization and many-body revivals from mixed phase space," Phys. Rev. X **10**, 011055 (2020).
[32] F. M. Surace, P. P. Mazza, G. Giudici, A. Lerose, A. Gambassi, and M. Dalmonte, "Lattice gauge theories and string dynamics in rydberg atom quantum simulators," Phys. Rev. X **10**, 021041 (2020).
[33] G. Magnifico, M. Dalmonte, P. Facchi, S. Pascazio, F. V. Pepe, and E. Ercolessi, "Real time dynamics and confinement in the $\mathbb{Z}_n$ schwinger-weyl lattice model for 1+ 1 qed," Quantum **4**, 281 (2020).
[34] T. Iadecola, M. Schecter, and S. Xu, "Quantum many-body scars from magnon condensation," Phys. Rev. B **100**, 184312 (2019).
[35] C. J. Turner, J.-Y. Desaules, K. Bull, and Z. Papić, "Correspondence principle for many-body scars in ultracold rydberg atoms," Phys. Rev. X **11**, 021021 (2021).
[36] D. Yuan, S.-Y. Zhang, Y. Wang, L.-M. Duan, and D.-L. Deng, "Quantum information scrambling in quantum many-body scarred systems," Phys. Rev. Research **4**, 023095 (2022).
[37] L. Pan and H. Zhai, "Composite spin approach to the blockade effect in rydberg atom arrays," Phys. Rev. Research **4**, L032037 (2022).
[38] K. Omiya and M. Müller, "Quantum many-body scars in bipartite rydberg arrays originating from hidden projector embedding," Phys. Rev. A **107**, 023318 (2023).
[39] K. Bull, I. Martin, and Z. Papić, "Systematic construction of scarred many-body dynamics in 1d lattice models," Phys. Rev. Lett. **123**, 030601 (2019).
[40] A. Hudomal, I. Vasić, N. Regnault, and Z. Papić, "Quantum scars of bosons with correlated hopping," Commun. Phys. **3**, 1 (2020).
[41] S. Scherg, T. Kohlert, P. Sala, F. Pollmann, B. H. Madhusudhana, I. Bloch, and M. Aidelsburger, "Observing non-ergodicity due to kinetic constraints in tilted fermi-hubbard chains," Nat. Commun. **12**, 1 (2021).
[42] J.-Y. Desaules, A. Hudomal, C. J. Turner, and Z. Papić, "Proposal for realizing quantum scars in the tilted 1d fermi-hubbard model," Phys. Rev. Lett. **126**, 210601 (2021).
[43] G.-X. Su, H. Sun, A. Hudomal, J.-Y. Desaules, Z.-Y. Zhou, B. Yang, J. C. Halimeh, Z.-S. Yuan, Z. Papić, and J.-W. Pan, "Observation of many-body scarring in a bose-hubbard quantum simulator," Phys. Rev. Research **5**, 023010 (2023).
[44] D. Banerjee and A. Sen, "Quantum scars from zero modes in an abelian lattice gauge theory on ladders," Phys. Rev. Lett. **126**, 220601 (2021).
[45] S. Biswas, D. Banerjee, and A. Sen, "Scars from protected zero modes and beyond in $u(1)$ quantum link and quantum dimer models," SciPost Phys. **12**, 148 (2022).
[46] J.-Y. Desaules, D. Banerjee, A. Hudomal, Z. Papić, A. Sen, and J. C. Halimeh, "Weak ergodicity breaking in the schwinger model," Phys. Rev. B **107**, L201105 (2023).
[47] J.-Y. Desaules, A. Hudomal, D. Banerjee, A. Sen, Z. Papić, and J. C. Halimeh, "Prominent quantum many-body scars in a truncated schwinger model," Phys. Rev. B **107**, 205112 (2023).
[48] P. Zhang, H. Dong, Y. Gao, L. Zhao, J. Hao, J.-Y. Desaules, Q. Guo, J. Chen, J. Deng, B. Liu, *et al.*, "Many-body hilbert space scarring on a superconducting processor," Nat. Phys. , 1 (2022).
[49] C.-J. Lin, A. Chandran, and O. I. Motrunich, "Slow thermalization of exact quantum many-body scar states under perturbations," Phys. Rev. Research **2**, 033044 (2020).
[50] F. M. Surace, M. Votto, E. G. Lazo, A. Silva, M. Dalmonte, and G. Giudici, "Exact many-body scars and their stability in constrained quantum chains," Phys. Rev. B **103**, 104302 (2021).
[51] I. Mondragon-Shem, M. G. Vavilov, and I. Martin, "Fate of quantum many-body scars in the presence of disorder," PRX Quantum **2**, 030349 (2021).
[52] K. Huang, Y. Wang, and X. Li, "Stability of scar states in the two-dimensional pxp model against random disorder," Phys. Rev. B **104**, 214305 (2021).
[53] M. Schecter and T. Iadecola, "Many-body spectral reflection symmetry and protected infinite-temperature degeneracy," Phys. Rev. B **98**, 035139 (2018).
[54] V. Karle, M. Serbyn, and A. A. Michailidis, "Area-law entangled eigenstates from nullspaces of local hamiltonians," Phys. Rev. Lett. **127**, 060602 (2021).
[55] W. Buijsman, "Number of zero-energy eigenstates in the pxp model," Phys. Rev. B **106**, 045104 (2022).
[56] T. Iadecola and M. Schecter, "Quantum many-body scar states with emergent kinetic constraints and finite-entanglement revivals," Phys. Rev. B **101**, 024306 (2020).
[57] R. Orús, "A practical introduction to tensor networks: Matrix product states and projected entangled pair states," Ann. Phys. (Amsterdam) **349**, 117 (2014).
[58] J. I. Cirac, D. Pérez-García, N. Schuch, and F. Verstraete, "Matrix product states and projected entangled pair states: Concepts, symmetries, theorems," Rev. Mod. Phys. **93**, 045003 (2021).
[59] S. Moudgalya, E. O'Brien, B. A. Bernevig, P. Fendley, and N. Regnault, "Large classes of quantum scarred hamiltonians from matrix product states," Phys. Rev. B **102**, 085120 (2020).
[60] S. R. White, "Density matrix formulation for quantum renormalization groups," Phys. Rev. Lett. **69**, 2863 (1992).
[61] U. Schollwöck, "The density-matrix renormalization group in the age of matrix product states," Ann. Phys. (Amsterdam) **326**, 96 (2011).
[62] V. Khemani, F. Pollmann, and S. L. Sondhi, "Obtaining highly excited eigenstates of many-body localized hamiltonians by the density matrix renormalization group approach," Phys. Rev. Lett. **116**, 247204 (2016).
[63] D. M. Kennes and C. Karrasch, "Entanglement scaling of excited states in large one-dimensional many-body localized systems," Phys. Rev. B **93**, 245129 (2016).
[64] S. P. Lim and D. N. Sheng, "Many-body localization and transition by density matrix renormalization group and exact diagonalization studies," Phys. Rev. B **94**, 045111 (2016).
[65] X. Yu, D. Pekker, and B. K. Clark, "Finding matrix product state representations of highly excited eigenstates of many-body localized hamiltonians," Phys. Rev. Lett. **118**, 017201 (2017).
[66] M. Serbyn, A. A. Michailidis, D. A. Abanin, and Z. Papić, "Power-law entanglement spectrum in many-body localized phases," Phys. Rev. Lett. **117**, 160601 (2016).
[67] D. J. Luitz, N. Laflorencie, and F. Alet, "Many-body localization edge in the random-field Heisenberg chain," Phys. Rev. B **91**, 081103 (2015).
[68] See Supplementary Materials at [URL will be inserted by publisher] for details about the exact MPS representations, the DMRG-S algorithm and more numerical results, which further include Ref. [76–78].
[69] D. Jaksch, J. I. Cirac, P. Zoller, S. L. Rolston, R. Côté, and M. D. Lukin, "Fast quantum gates for neutral atoms," Phys. Rev. Lett. **85**, 2208 (2000).
[70] M. D. Lukin, M. Fleischhauer, R. Cote, L. M. Duan, D. Jaksch, J. I. Cirac, and P. Zoller, "Dipole blockade and quantum information processing in mesoscopic atomic ensembles," Phys. Rev. Lett. **87**, 037901 (2001).

[71] In these cases, the DMRG-S algorithm extracts the low-entanglement contribution to the hybridized scars from ED, similar to the FSA method in Ref. [27, 28], while the DMRG-S states have energy variances several orders of magnitude smaller than the FSA states [68]. Despite the hybridization, the nontrivial conclusions about the scarred dynamics drawn from the DMRG-S states are not affected [68].

[72] As long as the eigenenergy variances are small enough for the DMRG-S states, the $\Delta(t)$ dynamics computed by the DMRG-S eigenenergies will agree with the exact Hamiltonian evolution. We explicitly benchmark the observable dynamics for small system sizes in Fig. 2(e) and [68].

[73] $a_k = (-1)^k \sqrt{\left[\frac{s!}{k!(s-k)!}\right] \Big/ \left[\frac{(2s-1)!!}{(2k-1)!!(2s-2k-1)!!}\right]}$.

[74] M. Fishman, S. R. White, and E. M. Stoudenmire, "The ITensor Software Library for Tensor Network Calculations," SciPost Phys. Codebases , 4 (2022).

[75] https://github.com/zhangshy2017/DMRG-S.

[76] B. Bauer and C. Nayak, "Area laws in a many-body localized state and its implications for topological order," J. Stat. Mech. Theor. Exp. **2013**, P09005 (2013).

[77] M. Friesdorf, A. H. Werner, W. Brown, V. B. Scholz, and J. Eisert, "Many-body localization implies that eigenvectors are matrix-product states," Phys. Rev. Lett. **114**, 170505 (2015).

[78] R. Reuvers, "An algorithm to explore entanglement in small systems," Proc. R. Soc. A **474**, 20180023 (2018).